Published in final edited form as:
J Bone Miner Res. 2015 March ; 30(3): 550–562. doi:10.1002/jbmr.2374.

Connexin 43 Channels are Essential for Normal Bone Structure and Osteocyte Viability

Huiyun Xu, PhD[1,2,#], **Sumin Gu, MD**[2,#], **Manuel A. Riquelme, PhD**[2], **Sirisha Burra, PhD**[2], **Danielle Callaway, BS**[2], **Hongyun Cheng, BS**[2], **Teja Guda, PhD**[5], **James Schmitz, BS**[3], **Roberto J. Fajardo, PhD**[3], **Sherry L. Werner, MD**[4], **Hong Zhao, MS**[6], **Peng Shang, PhD**[1], **Mark L. Johnson, PhD**[6], **Lynda F. Bonewald, PhD**[6], and **Jean X. Jiang, PhD**[2,*]

[1]School of Life Sciences, Northwestern Polytechnical University, Xian, China

[2]Department of Biochemistry, University of Texas Health Science Center at San Antonio, Texas

[3]Department of Orthopedics, University of Texas Health Science Center at San Antonio, Texas

[4]Department of Pathology, University of Texas Health Science Center at San Antonio, Texas

[5]Department of Biomedical Engineering, University of Texas at San Antonio, Texas

[6]Department of Oral Biology, School of Dentistry, University of Missouri, Kansas City, MO

Abstract

Connexin (Cx) 43 serves important roles in bone function and development. Targeted deletion of Cx43 in osteoblasts or osteocytes leads to increased osteocyte apoptosis, osteoclast recruitment, and reduced biomechanical properties. Cx43 forms both gap junction channels and hemichannels, which mediate the communication between adjacent cells or between cell and extracellular environments, respectively. Two transgenic mouse models driven by a DMP1 promoter with the overexpression of dominant negative Cx43 mutants were generated to dissect the functional contribution of Cx43 gap junction channels and hemichannels in osteocytes. The R76W mutant blocks gap junction channel, but not hemichannel function, and the Δ130-136 mutant inhibits activity of both types of channels. Δ130-136 mice showed a significant increase in bone mineral density compared to WT and R76W mice. MicroCT analyses revealed a significant increase in total tissue and bone area in midshaft cortical bone of Δ130-136 mice. The bone marrow cavity was expanded, whereas the cortical thickness was increased and associated with increased bone formation along the periosteal area. However, there is no significant alteration in the structure of trabecular bone. Histologic sections of the midshaft showed increased apoptotic osteocytes in Δ130-136, but not in WT and R76W, mice which correlated with altered biomechanical and estimated bone material properties. Osteoclasts were increased along the endocortical surface in both transgenic mice with a greater effect in Δ130-136 mice which likely contributed to the

* Address correspondence to Jean X. Jiang, jiangj@uthscsa.edu Address: Department of Biochemistry, University of Texas Health Science Center, 7703 Floyd Curl Drive, San Antonio, TX 78229-3900, USA.
# H.X. and S.G contributed equally to this work.

Authors' roles: Study design: HX, SG, MAR, SB, DC, TG, RF, SLW, LFB, JXJ. Study conduct: HX, SG, MAR, SB, DC, HC, TG, JS, HZ. Data collection: HX, SG, MAR, SB, DC, HC, TG, JS, HZ. Data analysis: HX, SG, MAR, SB, DC, TG, RF, SLW, MLJ, JXJ. Data interpretation: HX, SG, MAR, SB, DC, TG, RF, SLW, MLJ, LFB, JXJ. Drafting manuscript: HX, GS, BFB, RF, SLW, PS, LFB, JXJ. Revising manuscript content: GS, MAR, RF, JXJ. Approving final version of manuscript: HX, SG, RF, SLW, JXJ. JXJ takes responsibility for the integrity of the data analysis.

increased marrow cavity. Interestingly, the overall expression of serum bone formation and resorption markers were higher in R76W mice. These findings suggest that osteocytic Cx43 channels play distinctive roles in the bone; hemichannels play a dominant role in regulating osteocyte survival, endocortical bone resorption and periosteal apposition, and gap junction communication is involved in the process of bone remodeling.

INTRODUCTION

Bone tissue continuously undergoes remodeling through bone formation by osteoblasts and bone resorption by osteoclasts. The osteocyte has recently been postulated as the center of bone remodeling by orchestrating osteoblast and osteoclast functions (1,2). Osteocytes are embedded inside the bone mineral matrix, and long dendritic processes of osteocytes form a network connecting neighboring osteocytes and cells on the bone surface, such as osteoblasts and osteoclasts (3). Gap junction channels formed by Cx43 mediate cell-cell coupling of adjacent osteocytes and osteocytes with cells on the bone surface. Hemichannels are abundantly located on the cell surface of osteocytes and mediate the communication between the interior of the cell and its external environment (4-7). These connexin-based channels exhibit low substrate selectivity and permit small molecules (≤ 1 kDa) to pass through (8).

Mouse studies have shown that Cx43 plays important roles in bone growth, remodeling and survival of osteocytes (9-11). Conventional Cx43 knockout mice die prenatally (12); however, impaired differentiation of isolated osteoblasts is observed (13). Cx43 deletion driven by the α1 collagen (Col1A1) promoter results in low bone mineral density (BMD), thin cortical bone, decreased bone strength and an attenuated response to parathyroid hormone and mechanical loading (9,10,14). Cx43 deletion in more mature osteoblasts using the human osteocalcin (OCN)-driven promoter shows no abnormalities in bone mass (15), which is different from a more recent study showing a slightly lower BMD at 8-weeks old of age with increased osteoclastogenesis (11). Heterozygous gene knock-in (+/G138R) mice in osteoblasts with reduced gap junction communication develop osteopenia (16), while the global Cx43 G60S mutation with dominate negative effect on gap junctions displays early-onset osteopenia and abrogation of aged-related bone loss at a later stage (17,18). Deletion of Cx43 in osteocytes using the 8 kb DMP1 promoter leads to increased apoptotic osteocytes, endocortical bone resorption, and periosteal bone formation (19). Cell-based studies suggested that hemichannels are responsive to mechanical stimulation, resulting in the opening of these channels, and the release of factors including prostaglandins and ATP (6,20,21). These released extracellular factors are known to regulate bone metabolism (22-24).

In published knockout mouse studies, Cx43 has been deleted in both osteoblasts and osteocytes or primarily osteocytes alone. Since Cx43 is capable of forming both gap junction channels and hemichannels, it is not clear if the phenotypes observed in knockout models can be attributed to the impairment of either or both types of the channels. In the present study, we examined the functions of gap junction communication and hemichannels formed by Cx43 by generating two transgenic mouse models: R76W which has blocked gap

junction channels, but not hemichannels and Δ130-136 which has both channels inhibited. We determined the impact of the impairment of gap junction communication and/or hemichannels on bone mass, bone material and mechanical properties, osteocyte viability, bone formation and resorption. The skeletal phenotype of Δ130-136 mice was significantly different than the wild-type (WT), including increased BMD, enlarged midshaft cortical bone, greater osteocyte apoptosis and poorer material properties, whereas R76W mice had milder phenotypes with the increased serum markers for bone remodeling. The latter alterations were not observed in WT and Δ130-136 mice. Our findings suggest that Cx43 hemichannels are important in maintaining BMD, cortical bone structure/strength, osteocyte viability, periosteal bone formation and endocortical osteoclast numbers and activity; impairment of gap junction channels appears to have some effects on endocortical osteoclast numbers and activity, and periosteal bone formation and the expression of bone remodeling markers.

MATERIALS AND METHODS

Generation of two lines of transgenic mice expressing dominant negative mutants of Cx43

Transgenic mice overexpressing Cx43 mutants, R76W and Δ130-136, were generated. The DNA constructs were driven by a 10 kb-DMP1 promoter that leads the gene expression predominantly in the osteocytes (25). The 10-kb DMP1 promoter in pBluScript plasmid was generously provided by Dr. Stephen Harris at the University of Texas Health Science Center at San Antonio (UTHSCSA). Both mutants were cloned downstream of an intron sequence, and the 3' end of Cx43 cDNA was linked with a sequence of GFP cDNA. After generation and verification of DNA constructs, the transgenic mice were generated by the Transgenic Core Facility at the University of Texas Southwestern Medical Center. The genotyping was performed by PCR using genomic DNA isolated from mouse tails. Two pairs of the primers were used for genotyping of the transgenic mice (Table 1, Trans-F and TransG-R; and mCx43 S-F and mCx43 S-R). PCR primers were synthesized and constructs were sequenced at the University of Texas Health Science Center at San Antonio DNA Core Facility. All animal protocols were approved by the UTHSCSA Institutional Animal Care and Use Committee.

Isolation of RNA and protein samples from bone tissues, real-time PCR and western blotting

The long bone tissues of 4-month-old mice were isolated free of soft tissues, and bone marrow was removed by flushing with PBS. The bone samples were then pulverized using a frozen mortar and pestle in liquid nitrogen. Total RNA was extracted using TRI REAGENT® (Molecular Research Center, Inc. Cincinnati, OH) according to the manufacturer's instructions. The membrane protein lysates were prepared as following: pulverized bone tissue was homogenized with cold lysis buffer (5 mM Tris, 5 mM EDTA, 5 mM EGTA, and proteinase inhibitors). The bone lysates were centrifuged at 120000 X g for 45 min at 4°C, the pellet was resuspended in lysis buffer and the membrane protein was dissolved by addition of SDS to a 2% final concentration. The protein concentrations of SDS-dissolved lysates were determined by Micro BCA™ Protein Kit (Thermo Scientific, Rokckford, IL) and the lysates were used for western blotting analysis. To determine the

gene copy numbers of transgenic mice, mouse tail genomic DNAs were isolated following a previous published method (26, 27). Two pairs of primers were synthesized: mCx43 1201F and mCx43 1310R; and mCx50, 1272F and mCx50 1384R (Table 1). One pair, Cx50 mouse 1272F and mCx50 1384R (Table 1), was used to amplify mouse Cx50 gene as a reference. The other pair, mCx43 1201F and mCx43 1310R, was used for amplification of wild-type and transgenic Cx43 gene. Real time PCR was performed using ABI 7900 PCR device (Applied Biosystems®, Life Technologies, Carlsbad, CA) and SYBR Green (Life Technologies) with two step protocol (94°C, 10 sec and 65°C, 30 sec). ddCT method was used for qPCR data analysis. Real-time RT-PCR was performed to detect the mRNA expression of OPG and RANKL in bone using ABI 7900 PCR device and SYBR Green. The primers for OPG (OPG-F and OPG-R) and RANKL (RANKL-F and RANKL-R) are listed in Table 1. GAPDH was used as a housekeeping gene control. Western blotting was performed to detect the expression of GFP-connexin in the bone lysates by probing with rabbit anti-GFP anti-antibody of (1:1000 dilution) or mouse anti-β-actin (1:5000), and followed by secondary HRP-conjugated anti-rabbit or anti-mouse secondary antibody (1:5000), respectively.

Isolation of primary osteocytes from mice long bone

The preparation of enriched primary osteocytes was based on a previously published protocol (28). Briefly, long bones were dissected from 2-3-week-old mice and bone marrow was removed by flushing with PBS. The bones were cut into pieces ranging 1.5 to 2 mm in length and digested by alternate uses of collagenase type I (Sigma) and EDTA on a rotating shaker in a CO_2 incubator at 37°C. After multiple treatments with collagenase type I and EDTA to remove fibroblasts, osteoblasts and other lining cells, the final digests are enriched for osteocytes. The released osteocytes were collected, strained through a 70 μm mesh cell strainer and plated on collagen-coated dish in α-MEM (Life Technologies) with 5% FBS +5% BCS (Hyclone, Logan, UT).

Hemichannel dye uptake and gap junction coupling assays

A subset of the isolated primary osteocytes was seeded in collagen-coated coverslips mounted in the Focht Chamber System 2 (FCS2) (Bioptechs, Butler, PA). The cells where subjected to flow shear stress (FSS) at 4 dynes/cm^2 for 15 min in the presence of 25 μM ethidium bromide (EtBr) in the recording media (HCO^{3-} -free αMEM medium buffered with 10 mM HEPES). The FSS chamber was placed on the stage of a Nikon Eclipse TE 200 microscope. The fluorescence images were captured every 30 sec at the excitation wavelength of 561 nm. The intensity of EtBr fluorescence in cells was measured and quantified by Image J software. Primary osteocytes were microinjected using an Eppendorf micromanipulator InjectManNI 2 and Femtojet (Eppendorf) at 37°C with 10 mM Alexa594 dye in PBS for 5 min to examine gap junction cell coupling, which was observed under an inverted microscope equipped with Lambda DG4 device (Sutter instrument CO, Novato CA) with mercury arc lamp illumination and a Nikon eclipse (Nikon, Japan) using a rhodamine filter.

BMD measurement

Mice were anesthetized by intraperitoneal injection of 80 mg/kg of ketamine (Butler Schein, Dublin, OH) with 10 mg/kg of xylazine (Butler Schein). The BMD was measured once a month in all male mice from 1-4-months of age using a dual-energy X-ray absorptiometry (DEXA) scanner (Lunar PIXImus Densitometer, GE Medical Systems, Piscataway, NJ). The BMD of the spine, tibia, femur and a total bone measurement were acquired.

MicroCT analysis

The 4-month-old male mice were sedated under isoflurane (Baxter, Deerfield, IL) and sacrificed by cervical dislocation. Tibias from 4-month-old male WT and transgenic mice were isolated. The structural properties of cortical and trabecular bones were evaluated using a desktop microCT imaging system (Brüker SkyScan 1173, Kontich, Belgium). Samples were scanned in saline with the following settings: 60 kV, 167 μA beam intensity, 0.5 mm aluminum filter, 0.7° rotation step, 4 frame averaging, 1090 ms integration time, 1024 × 1024 pixel matrix, and a 10 μm isotropic voxel dimension. After scanning, noise was removed from the images by eliminating disconnected objects smaller than 4 pixels in size. Two volumes of interest were selected in the metaphyseal and midshaft regions and automated contouring was used to delineate cortical and trabecular bone regions. In the proximal tibial metaphysis, the trabecular bone volume of interest (VOI) was positioned 50 slices distal to the proximal growth plate and extended 150 slices in the distal direction. The VOI conformed to the endocortical boundary. An appropriate and uniform threshold was applied to all specimens after comparing grayscale and binarized images in both groups. For trabecular bone, a grayscale value of 80 in a set of 8-bit slices was set as the threshold. After thresholding, the BV/TV (%), Tb.Th (mm), Tb.Sp (mm) and Tb.N (mm^{-1}) were quantified (29,30). Cortical bone structure was analyzed over 50 slices centered at the 55% of length (from proximal to distal) position in the tibial diaphysis. We used the 55% length from the proximal end because the linea aspera of the mouse influenced the shape less. This ridge is one of the insertion sites of the gluteal musculature and it contributes to an odd shape of the femur shaft. We treated all groups similarly. Grey values of 106 and 256 were set as the window for cortical bone. Cortical bone analyses included the diaphyseal total area (Tt.Ar, mm^2), bone area (Ct.Ar, mm^2), and the area moments of inertia (MMI).

Bone material and biomechanical properties

Femur bones were removed from 4-month-old male, WT and transgenic mice, and soft tissues were removed. Bones were kept fresh-frozen in saline soaked gauze at −20°C until three point bending tests were performed. These tests were performed on an MTS Insight 5 Electromechanical system (MTS Systems Corporation, Eden Prairie, MN) using TestWorks software (version 4.0). The span distance for the 3 point bending test was 8 mm and the loading pin was placed at the mid-point of the span. The test was performed in displacement control mode at a constant rate of 0.5 mm/sec with data collected at a 200 Hz sampling rate for all measurements. Stress calculations were performed by taking into account the accurate cross sectional areas and moments of inertia of each individual sample determined from microCT.

TUNEL, Histology, immunohistochemistry and histomorphometric Analysis

The In Situ Cell Death Detection Kit, TMR red® (Roche, Pleasanton, CA) was used for detection and quantification of bone cell apoptosis following manufacture's instruction. Briefly, paraformaldehyde fixed bone tissue sections were treated with proteinase K in Tris buffer containing 0.1% Triton X-100 and broken DNAs were labeled with TUNEL reaction mixture of reagent. The sections were analyzed and photographed using an Olympus 1X70 microscope (Olympus, Japan), and the number of apoptotic cells was counted. For preparation of paraffin sections, the tibial bones from 4-month-old male mice were fixed in 4% paraformaldehyde for 2 days prior to decalcification with 10% EDTA (pH 7.5) for 6 weeks. The samples were embedded in paraffin and 7 μm thick sections were cut onto glass slides and stained with hematoxylin and eosin (H&E). The numbers of empty and total osteocytic lacunae were quantified. To detect cleaved caspase-3, paraffin sections were first labeled with anti-cleaved caspase-3 antibody (1:800 dilution) (Cell Signaling Technology, Danvers, MA) and followed by anti-rabbit VECTASTAIN® ABC kit according to the manufacturer instructions (Vector, Burlingame, CA). Tissue sections were TRAP stained using Leukocyte Acid Phosphatase Staining Kit (Sigma. St. Louis, MO) according to the manufacturer's protocols. Bioquant Image Analysis System software (BIOQUANT Image Analysis, Nashville, TN) was used to determine osteoclast number (Oc.N), osteoblast number (Ob.N) and bone surface (BS) in the metaphyseal trabecular bone and along the endocortical surface from the metaphysis to the upper midshaft. The Ob.N/BS and Oc.N/BS were then calculated.

Calcein labeling and dynamic bone histomorphometry

Fifteen-week-old mice were given an intraperitoneal injection of calcein (Sigma) at 30 mg/kg body weight and followed by the second injection 10 days later. Four days after the second injection the mice were sacrificed, and tibias were dissected and embedded undecalcified in methylmethacrylate for plastic sections. Digital images were obtained using a fluorescence microscope (Olympus). The following bone parameters were quantified in the trabecular bone, periosteal and endocortical regions with Bioquant Imaging software: total perimeter (BS); single label perimeter (sLS); double label perimeter (dLS) and double label area (dL.Ar) The following values were then calculated: mineralizing surface (MS/BS = [1/2sLS+dLS]/BS), mineral apposition rate (MAR =dL.Ar/dLS/10) and bone formation rate (BFR/BS=MAR×(sLS/2+dLS)/BS).

Primary osteoclast culture, and determination of TRAP staining and TRAP activity

Primary bone marrow cells were isolated according to standard protocols. In brief, bone marrow was collected by washing the marrow cavity with cell culture media delivered via a 21G needle. In order to assess the impact of stromal cells on osteoclast differentiation, a portion of total marrow was plated into 48 well plates with 30 ng/mL CSF-1 (R&D Systems, Minneapolis, MN) and 10 ng/ml RANKL (R&D Systems) for a total of 4 days after which cells were either fixed and stained or assessed for TRAP activity. The remaining marrow was cultured overnight after which the non-adherent fraction was collected. All cells were grown in αMEM (Life Technologies) with 10% FBS (Biosera, Kansas City, MO) and antibiotics. The non-adherent cells were allowed to expand for 3 days in 30 ng/ml CSF-1.

Bone marrow macrophages were next collected and plated with 30 ng/ml CSF-1 and 10 ng/ml RANKL, and allowed to differentiate into osteoclasts. TRAP staining was performed with the leukocyte acid phosphatase kit (Sigma) according to the manufacturer's protocols. To measure TRAP activity, live bone marrow cells in a 48-well plate were incubated for 30 min at 37°C in a pre-warmed solution containing 4% acetate, 4% tartrate, 0.1% sodium dodecyl sulfate, and 6 tablets of SIGMA FAST™ p-nitrophenyl phosphate (Sigma). The resulting supernatant was transferred to a fresh 96 well plate and read at 405 nm on a BioRAD iMark Microplate Reader (Bio-Rad Laboratories, Hercules, CA). Total numbers of TRAP-positive multi-nucleated (>3) cells (MNCs) were quantified.

Quantification of serum biomarkers of bone formation and resorption

Sera were collected from 4-month-old mice after fasting overnight. Serum bone biomarkers, type I collagen N-terminal propeptide (PINP) and C-terminal telopeptides (CTX) were measured with ELISA kits from Immunodiagnostic Systems (Fountain Hills, AZ) according to manufacturer's protocols.

Statistical analysis

Statistical analysis was performed using GraphPad Prism 5 statistics software (GraphPad). All data were expressed as mean ± standard derivation (SD). One-way ANOVA with Tukey test was used for statistics analysis. Asterisks indicate the degree of significant differences compared with the controls (*, $P < 0.05$; **, $P < 0.01$; ***, $P < 0.001$).

RESULTS

Generation of two transgenic mice expressing dominant negative Cx43 mutants that differentially inhibits gap junction channels and hemichannels

We took advantage of two previously characterized dominant negative mutants, R76W and Δ130-136 to dissect the distinct functions of Cx43-forming gap junction channels and hemichannels. The Arg-76 residue located in the interface of the second transmembrane and first extracellular loop domains is highly conserved across connexin isoforms and animal species. The mutation of R75 of Cx26, the conserved residue corresponding to R76 of Cx43, has been demonstrated to have a dominant negative effect on gap junction channels, but not hemichannels (31). A deletion mutation in the intracellular loop domain of the amino acid residues 130 to 136 is reported to have a dominant negative effect on both gap junction channels and hemichannels (32) (Fig. 1A). The DNA constructs used to generate transgenic mice contain the 10-kb DMP1 promoter and the exon 1 (E1) of DMP1, which are connected with Cx43 negative mutants and GFP with an intron (Fig. 1B). The gene insertion of these two mutants was detected by PCR using specific primers (Fig. 1C). Real time PCR showed similar numbers of relative copy numbers of gene insertion in these two transgenic mice (Fig. 1D). The protein expression of these two mutants was shown by western blotting of membrane extracts of the bone lysates (Fig. 1E). We determined the dominant negative effect of these mutants on channels in primary osteocytes isolated from these two transgenic mice. Gap junction channels and hemichannels were assayed using dye coupling (Fig. 1F) and dye uptake (Fig. 1G), respectively. The osteocytes expressing either Δ130-136 or R76W mutants failed to couple with surrounding cells based on Alexa594 signals through gap

junction channels as compared to those isolated from WT mice (Fig. 1F). Hemichannels are known to open in response to mechanical stimulation (6). In the presence of flow shear stress (FSS) increased EtBr uptake indicated that WT and R76W hemichannels in osteocytes isolated from WT and R76W mice were open compared to non-FSS controls (Fig. 1G). EtBr uptake was similar between non-FSS and FSS in Δ130-136 mice, indicating that the channels were not open. Additionally, the hemichannel activity was higher in osteocytes from R76W mice among FSS-treated mice. These results showed that osteocytes expressing mutant, Δ130-136 or R76W in transgenic mice exhibited dominant negative effects on gap junction channels and hemichannels or only on gap junction channels, respectively.

Altered skeletal phenotypes in Cx43 transgenic mice

A significant increase of BMD was observed in the total body, spine, tibial, and femur measurements of Δ130-136 mice at each age (1-4 months) compared to the WT (Fig. 2) and the difference between WT and Δ130-136 mice becomes more apparent in spine, tibia and femur with the age. BMD values of R76W mice were similar to WT mouse. The coefficient of variations was calculated with the value of 98%.

MicroCT analysis indicated that tibial proximal metaphysis trabecular bone volume fractions (BV/TV) (Fig. 3A), thicknesses (Tb.Th) (Fig. 3B) and numbers (Tb.N) (Fig. 3C) were similar across groups. However, significant changes were observed in midshaft cortical bones. The Δ130-136 had a significantly higher total area (Fig. 3D) and bone area (Fig. 3E) compared to the WT and R76W mice. The bone area fraction by the ratio of bone area vs. tissue area of the midshaft in Δ130-136 was, however; significantly lower than the other two groups (Fig. 3F). The thickness of the cortical wall was higher in the Δ130-136 mice compared to the WT (Fig. 3G). Interestingly, the mean polar moment of inertia (MMI) was dramatically increased in Δ130-136 mice as a result of a cortex that was distributed further from the center of the bone (Fig. 3H). The enlarged bone marrow cavity was also observed by micro-CT imaging of the cross-sections of midshaft tibial bone (Fig. 3I). Moreover, the shape of the bone marrow cavity appeared to be irregular and the endocortical surface of the bone in Δ130-136 mice was less smooth as compared to WT and R76W mice. These data suggest an endocortical resorption and a periosteal expansion of midshaft cortical bone in Δ130-136 mice. Interestingly, microCT results in Δ130-136 mice are similar to previous reported data of Cx43 conditional knockout mice with DMP-1 promoter (33). However, compared to WT mice, significant alteration was not observed in R76W mice for both trabecular and cortical bone.

Consistent with the data obtained from tibial midshaft bone, microCT analysis of femur cortical bones of Δ130-136 mice showed a significant increase in total tissue area (Fig. 4A), bone area (Fig. 4B) and MMI (Fig. 4C) compared to WT and R76W mice. Three point bending analyses revealed non-signficant differences in stiffness in all groups (Fig. 4D). Yield force (Fig. 4E) was significantly increased in Δ130-136 compared to the other two groups. Interestingly, Δ130-136 mice had significantly lower material properties of elastic modulus (Fig. 4F) and fracture strength (Fig. 4G). In addition, we also measured post-yield toughness and post-yield displacement. Post-yield toughness was lower in the Δ130-136 group (3610 ± 2818 MPa) compared to the WT (5866 ± 2363 MPa) and R76W (6682 ±

1304 MPa) groups. Post-yield displacement was also reduced in the Δ130-136 group (0.378 ± 1.310 mm) compared to the WT (0.676 ± 0.328 mm) and R76W (0.762 ± 0.228 mm) groups. The data are presented as mean ± SD, n = 3. The WT and R76W groups were similar in all estimated material properties comparisons. These studies showed that although the structural properties of the cortical bone were greater in Δ130-136 mutant, the mutant had reduced bone material properties.

Expression of Δ130-136 significantly increases cortical osteocyte apoptosis and death with empty lacunae

Histological analysis showed an increase in the numbers of empty lacunae in cortical bones of Δ130-136 mice (indicated by arrowheads), but the presence of empty lacunae in WT and R76W mice is minimal (Fig. 5A). In addition, compared to those in WT and R76W mice, cortical bone sections in Δ130-136 mice were unevenly and also lightly stained by H&E. These results indicate relatively disorganized matrix structure with lesser amount of proteins. We analyzed apoptotic osteocytes using TUNEL staining (Fig. 5, B and C) and the numbers of cells expressing cleaved (active) caspase-3 (Fig. 5D). As shown in cortical bone (corti.) regions of WT and transgenic mice, there was an increase of TUNEL labeling (red) in osteocytes in Δ130-136 compared to WT and R76W mice (Fig. 5B). The similar levels of TUNEL-positive signals were consistently observed in bone marrow regions of WT as well as transgenic mice, which further support the specificity of transgenic expression in osteocytes. The quantification of TUNEL-positive osteocytes confirmed the significant increase of osteocytes undergoing apoptosis in Δ130-136 mice (Fig. 5C). Immunohistochemical labeling with anti-cleaved caspase-3 antibody showed an increase of numbers of cleaved caspase-3-positive cells (Fig. 5D), further demonstrating the increase of apoptotic osteocytes in the cortical bone with the expression of the Δ130-136 mutant.

Impairment of Cx43 channels affects osteoblasts and osteoclasts, and the rate of bone formation and remodeling

The osteoblast numbers were not significantly altered in trabecular bone (Fig. 6A) and endocortical bone of transgenic mice (Fig. 6B) in all groups. Although there was no significant difference in osteoclast numbers in trabecular bone of Δ130-136 mice (Fig. 6C), the number of osteoclasts along the endocortical bone was significantly increased in Δ130-136 mice (Fig. 6D). Interestingly, endocortical osteoclast numbers in R76W mice were significantly increased (Fig. 6D). Consistently, the number of osteoclasts isolated from the bone marrow are significantly higher in both R76W and Δ130-136 mice (Fig. 6E). These data suggest that gap junction channels in osteocytes influence the numbers and activities of osteoclasts.

The rate of bone formation was measured by dynamic histomorphometry via calcein injection and double labeling assay. Interestingly, increased bone formation as indicated by the bone formation rate (BFR/BS) (Fig. 7A) and mineral apposition rate (MAR) (Fig. 7B) were seen in trabecular bone of Δ130-136 mice as compared to R76W and WT mice. The ratio of mineral surface vs. bone surface was similar in all groups (Fig. 7C). Notably, a significant increase of BFR/BS, MAR and MS/BS was observed in midshaft periosteal bone of Δ130-136 mice (Fig. 7, D-G), which likely accounted for the increased midshaft cortical

bone demonstrated by microCT. An increase in midshaft periosteal BFR and MAR was also seen in R76W mice (Fig. 7, E and F). In contrast, bone formation parameters along endocortical bone in transgenic mice were not different from those in WT mice (Fig. 7, H-K). Together, these data suggest that impairment of Cx43 channels influences endocortical bone resorption and periosteal bone apposition with more profound impact observed in Δ130-136 mice.

To dissect the underlying mechanism of the alteration of osteoblast and osteoclast activities, we examined the expression of bone remodeling markers. Osteoprotegerin (OPG) is an osteoclastogenesis inhibitor and a decoy receptor for the receptor activator of nuclear factor kappa B ligand (RANKL). In contrast to OPG, RANKL activates osteoclasts through the activation of the osteoclast's RANK receptor. Interestingly, the mRNA levels of both OPG and RANKL levels were significantly reduced in bone tissues of Δ130-136 mice as compared to WT controls (Fig. 8, A and B), whereas the ratio of RANK/OPG mRNA was significantly reduced only in R76W mice. To further determine overall process of bone turnover, we measured the serum contents of two biochemical markers of bone remodeling; PINP and CTX. The elevated levels of PINP and CTX indicate the increase of overall bone formation and resorption, respectively. Interestingly, both PINP and CTX levels were significantly enhanced in R76W mice as compared to WT and Δ130-136 mice (Fig. 8, C and D). These results suggest that hemichannels have major impacts on the expression of OPG and RANKL. However, gap junction communication is involved in expression of bone remodeling markers for bone formation and resorption.

DISCUSSION

In this study, we used two transgenic mouse models expressing dominant negative mutants of Cx43 to determine the specific function of gap junction channels and hemichannels. These dominant negative mutants acted as expected in primary osteocytes from transgenic mouse lines by specifically inhibiting gap junction channels and/or hemichannels formed by endogenous Cx43. We observed the significant changes on bone mass, structure, strength and osteocyte viability in Δ130-136 mice while the overall bone phenotype in R76W mice are relatively lesser evident with increased endocortical osteoclast numbers and activity and the expression of serum bone remodeling markers. Given that Δ130-136 inhibits both gap junction channels and hemichannels, but R76W only impairs gap junction channels, it suggests that Cx43 hemichannels in osteocytes are likely to play a predominant role in maintaining osteocyte viability that is essential for bone integrity and longevity. This *in vivo* evidence indicates the distinctive roles of Cx43 gap junction channels and hemichannels in the osteocytes.

Previous *in vitro* studies have shown that Cx43 hemichannels in osteocytes are involved in the transduction of cell survival signals in response to bisphosphonate treatment (34). Cx43 hemichannels in osteocytes are highly responsive to mechanical loading through the release of bone anabolic factors including prostaglandins and ATP in the cell culture system *in vitro* (6,21,35). Even under normal, static conditions, bone tissues in the body are continuously subject to mechanical stimulations derived from various sources including gravity (macroscopic) and blood circulation (microscopic). Therefore, Cx43 hemichannels in

osteocytes *in situ* are likely active in response to these stimuli. Impairment of Cx43 hemichannels would block the exchange of small signaling and other molecules between cytoplasm and extracellular environments. Moreover, the factors released by hemichannels are shown to function in an autocrine or paracrine fashion on osteocytes and other bone cells. We have shown earlier that hemichannels serve as a portal for the release of PGE_2 in response to mechanical stimulation in osteocytes (6). Moreover, in vitro studies reported that PGE_2 released by osteocytes mediated by Cx43 hemichannels protects osteocytes against glucocorticoid-induced osteocyte death (6,36). We observed here the significant increase of apoptotic osteocytes and empty lacunae only in Δ130-136, but not R76W mice. Thus, it is possible that reduced release of PGE_2 as a result of the impairment of Cx43 hemichannels may lead to the increased apoptosis of osteocytes in cortical bone. This study supports the notion that functional Cx43 hemichannels is involved in the survival of osteocytes in bone tissues. The presence of apoptotic osteocytes would undoubtedly compromise the bone quality and strength as observed in Δ130-136 mice.

The bone phenotypes exhibited by Δ130-136 mice with the impairment of both gap junction channels and hemichannels have some similarities to osteocyte-specific Cx43-deficient mice driven by 8-kb DMP1 promoter. Both 8-kb and 10-kb DMP1 promoters are reported to drive predominant gene expression in osteocytes and the specificity of these two promoters are comparable (37). In the study by Bivi et al. (33), they reported an increase of osteocyte apoptosis, higher marrow cavity, total tissue areas and periosteal bone formation rate at the femur mid-diaphysis in this animal model. Also consistent partially with our observation, there were no alterations in the endocortical bone formation rate, bone apposition rate and mineral surface. The increased osteoclast levels reported in Cx43 knockout mice were also seen in Δ130-136. However, in contrast to the lack of alterations in bone mass in the Cx43 knockout model, Δ130-136 mice have a significantly higher BMD associated with increased total tissue and bone volumes. Additionally, cortical thickness is significantly increased in Δ130-136 mice, which is not reported for Cx43 knockout mouse model (33). Some differences between the Cx43-deficient model and Δ130-136 transgenic model could be due to the fact that although Cx43 deletion abolishes both gap junction channel and hemichannel function, it also diminishes a significant amount of Cx43 retained in the cytoplasm of the osteocytes (5,38). Studies in our model suggest that decreased Cx43 gap junction and hemichannel expression impairs osteocyte survival/function and leads to enhanced osteoclastic endocortical bone resorption and osteoblastic periosteal bone formation, resulting in a net increase in the diameter of cortical bone.

In the Δ130-136 mice, prominent structural changes are observed in cortical, but not trabecular bone. Δ130-136 mice have enlarged bone marrow cavity largely caused by the decreased endosteal osteoblast numbers and increased osteoclast numbers. Moreover, cortical thickness is greater in Δ130-136 mice than WT and R76W mice. This increase is likely caused by even more periosteal bone apposition than endosteal bone resportion. These cortical bone changes give the Δ130-136 mice greater whole bone strength in 3 point bending because the bone tissue is positioned further away from the neutral axis of bending. However, once the 3 point bending was normalized by the cross-section, thereby giving the estimated material properties, we observed significantly weaker bone in Δ130-136 mice.

These data correlate with more apoptotic osteocytes and empty lacunae in this model. The observation of Δ130-136 mice associated with an enlarged marrow cavity is highly relevant to clinical osteoporosis where endocortical bone resorption is enhanced. Moreover, increased apoptotic osteocytes in this mouse model suggest that proper Cx43 hemichannel function may be important for ameliorating bone aging where increased osteocyte apoptosis leads to impaired bone strength.

OPG and RANKL are important regulators for bone modeling and remodeling (39). We observed the reduction of these two factors in Δ130-136, but lesser in R76W mice, especially the level of OPG. Since Δ130-136 transgenic mice have similar levels of reduction in both OPG and RANKL levels, the ratio of these two parameters is not significantly altered in comparison to WT mice. Interestingly, the ratio of RANKL to OPG was significantly reduced in R76W mice. Osteocytic Cx43 hemichannels are portals for the release of prostaglandins including prostaglandin E_2 (PGE_2) (6,35). Previous studies have shown that PGE_2 influences the levels of OPG and RANKL in osteoblasts and this effect is mediated in a dose-dependent manner (40-42). This may explain that disruption of Cx43 hemichannels in Δ130-136 mice, which may be associated with the reduced PGE_2 release, leads to the decreased levels of OPG and RANKL. Moreover, two recent studies reported that osteocytes are a major source in generating RANKL (43,44). Here we showed fewer osteocytes in Δ130-136 mice as evidenced by empty lacunae and more apoptotic osteocytes. Consistently, the production of RANKL by osteocytes is decreased in Δ130-136 mice.

The R76W mice with only the impairment of gap junction channels in osteocytes showed lesser degree of bone alterations as compared to Δ130-136 mice, likely due in part to normal osteocyte survival. Although there is no significant alteration in the phenotypes of tibial bone in R76W mice, the serum bone remodeling markers, PINP and CTX were elevated in R76W mice. The serum measurements for bone remodeling markers reflect the activities of the overall bone including both cortical and trabecular bone all over the body, not just tibial bone.. The intercellular communication mediated by gap junction channels with the exchange of molecules between osteocytes, and osteocytes and other bone cells could intricately control the growth and differentiation of osteoblasts and osteoclasts. Indeed, previous studies have shown the direct interacellular coupling between osteocytes and osteoblasts and this communication regulates osteoblast differentiation (45). It is plausible that gap junction channels and hemichannels work coordinately in modulating the bone remodeling. Under normal physiological situation, the well-balanced actions of both types of channels are the key to modulating bone remodeling. In addition, although we could not detect dramatic changes in bone structure and mass in R76W mice at the ages we examined, this does not exclude the possibility that the bone phenotype may be altered at older ages. Also, it would be of interest to determine whether anabolic mechanical loading is altered in these mice. These are the research directions warranting our further investigation. Together, this study overcomes the limitation in Cx43 gene deletion models and helps define the specific function and mechanism of osteocytic gap junction channels and hemichannels in osteocyte viability and the function of osteocytes in sustaining bone structure, strength and remodeling.

ACKNOWLEDGEMENTS

The authors would like to thank Dr. Stephen Harris at the UTHSCSA for providing a plasmid containing 10-kb DMP1, Ms. Diane Horn at UTHSCSA for plastic section preparation and bone histomorphormetry, and the members of Dr. Jiang's laboratory for critical reading of the manuscript.

The work was supported by NIH grants AR46798 to JXJ, LFB and MLJ, RR025687 and AG041505 to RJF and AG045040 to SW, Welch Foundation grant AQ-1507 to JXJ, China 973 Program (2011CB710903 to PS) and National Natural Science Foundation of China (31328016 to JXJ, PS, HX, and 31170812 to HX and JXJ).

References

1. Rochefort GY, Pallu S, Benhamou CL. Osteocyte: the unrecognized side of bone tissue. Osteoporos. Int. 2010
2. Bonewald LF. The amazing osteocyte. J Bone Miner. Res. 2011; 26:229–238. [PubMed: 21254230]
3. Bonewald LF. Generation and function of osteocyte dendritic processes. J. Musculoskelet. Neuronal Interact. 2005; 5:321–324. [PubMed: 16340122]
4. Kato Y, Windle JJ, Koop BA, Mundy GR, Bonewald LF. Establishment of an osteocyte-like cell line, MLO-Y4. J. Bone Miner. Res. 1997; 12:2014–2023. [PubMed: 9421234]
5. Cheng B, Zhao S, Luo J, Sprague E, Bonewald LF, Jiang JX. Expression of functional gap junctions and regulation by fluid flow shear stress in osteocyte-like MLO-Y4 cells. J. Bone Miner. Res. 2001; 16:249–259. [PubMed: 11204425]
6. Cherian PP, Siller-Jackson AJ, Gu S, Wang X, Bonewald LF, Sprague E, Jiang JX. Mechanical strain opens connexin 43 hemichannels in osteocytes: a novel mechanism for the release of prostaglandin. Mol. Biol. Cell. 2005; 16:3100–3106. [PubMed: 15843434]
7. Loiselle AE, Jiang JX, Donahue HJ. Gap junction and hemichannel functions in osteocytes. Bone. 2013; 54:205–212. [PubMed: 23069374]
8. Goodenough DA, Goliger JA, Paul DL. Connexins, connexons, and intercellular communication. Annu. Rev. Biochem. 1996; 65:475–502. [PubMed: 8811187]
9. Chung DJ, Castro CH, Watkins M, Stains JP, Chung MY, Szejnfeld VL, Willecke K, Theis M, Civitelli R. Low peak bone mass and attenuated response to parathyroid hormone in mice with an osteoblast-specific deletion of connexin43. J. Cell Sci. 2006; 119:4187–4198. [PubMed: 16984976]
10. Grimston SK, Brodt MD, Silva MJ, Civitelli R. Attenuated response to in vivo mechanical loading in mice with conditional osteoblast ablation of the connexin43 gene (Gja1). J. Bone Miner. Res. 2008; 23:879–886. [PubMed: 18282131]
11. Zhang Y, Paul EM, Sathyendra V, Davison A, Sharkey N, Bronson S, Srinivasan S, Gross TS, Donahue HJ. Enhanced Osteoclastic Resorption and Responsiveness to Mechanical Load in Gap Junction Deficient Bone. PLos One. 2011; 6:e23516. [PubMed: 21897843]
12. Reaume AG, De Sousa PA, Kulkarni S, Langille BL, Zhu D, Davies TC, Juneja SC, Kidder GM, Rossant J. Cardiac malformation in neonatal mice lacking connexin43. Science. 1995; 267:1831–1834. [PubMed: 7892609]
13. Lecanda F, Warlow PM, Sheikh S, Furlan F, Steinberg TH, Civitelli R. Connexin43 deficiency causes delayed ossification, craniofacial abnormalities, and osteoblast dysfunction. J. Cell Biol. 2000; 151:931–943. [PubMed: 11076975]
14. Grimston SK, Screen J, Haskell H, Chung DJ, Brodt MD, Silva MJ, Civitelli R. Role of connexin43 in osteoblast response to physical load. Ann. N. Y. Acad. Sci. 2006; 1068:214–224. [PubMed: 16831921]
15. Plotkin LI, Lezcano V, Thostenson J, Weinstein RS, Manolagas SC, Bellido T. Connexin 43 is required for the anti-apoptotic effect of bisphsphonates on osteocytes and osteoblasts in vivo. J. Bone Miner. Res. 2008; 23:1712–1721. [PubMed: 18597631]
16. Watkins M, Grimston SK, Norris JY, Guillotin B, Shaw A, Beniash E, Civitelli R. Osteoblast connexin43 modulates skeletal architecture by regulating both arms of bone remodeling. Mol. Biol. Cell. 2011; 22:1240–1251. [PubMed: 21346198]
17. Flenniken AM, Osborne LR, Anderson N, Ciliberti N, Fleming C, Gittens JE, Gong XQ, Kelsey LB, Lounsbury C, Moreno L, Nieman BJ, Petrson K, Qu D, Roscoe W, Shao Q, Tong D, Veitch

GI, Voronina I, Vukobradovic I, Wood GA, Zhu Y, Zirngibl RA, Aubin JE, Bai D, Bruneau BG, Grynpas M, Henderson JE, Kenkelman RM, McKerlie C, Sled JG, Stanford WL, Laird DW, Kidder GM, Adamson SL, Rossant J. A Gja1 missense mutation in a mouse model of oculodentodigital dysplasia. Development. 2005; 132:4375–4386. [PubMed: 16155213]

18. Zappitelli T, Chen F, Moreno L, Zirngibl RA, Grynpas M, Henderson JE, Aubin JE. The G60S connexin 43 mutation activates the osteoblast lineage and results in a resorption-stimulating bone matrix and abrogation of old-age-related bone loss. J Bone Miner. Res. 2013; 28:2400–2413. [PubMed: 23606335]
19. Bivi N, Condon KW, Allen MR, Farlow N, Passeri G, Brun LR, Rhee Y, Bellido T, Plotkin LI. Cell autonomous requirement of connexin 43 for osteocyte survival: consequences for endocortical resorption and periosteal bone formation. J. Bone Miner. Res. 2011; 27:374–389. [PubMed: 22028311]
20. Ajubi NE, Klein-nulend J, Nijweide PJ, Vrijheid-lammers T, Alblas MJ, Burger EH. Pulsating fluid flow increases prostaglandin production by cultured chicken osteocytes-a cytoskeleton-dependent process. Biochem. Biophy. Res. Comm. 1996; 225:62–68.
21. Genetos DC, Kephart CJ, Zhang Y, Yellowley CE, Donahue HJ. Oscillating fluid flow activation of gap junction hemichannels induces ATP release from MLO-Y4 osteocytes. J. Cell. Physiol. 2007; 212:207–214. [PubMed: 17301958]
22. Baylink TM, Mohan S, Fitzsimmons RJ, Baylink DJ. Evaluation of signal transduction mechanisms for the mitogenic effects of prostaglandin E2 in normal human bone cells in vitro. J. Bone Min. Res. 1996; 11:1413–1418.
23. Keller J, Klamer A, Bak B, Suder P. Effects of local prostaglandin E_2 on fracture callus in rabbit. Acta. Orthop. Scand. 1993; 64:59–63. [PubMed: 8451949]
24. Jee WSS, Ueno K, Deng YP, Woodbury DM. The effects of prostaglandin E2 in growing rats: increased metaphyseal hard tissue and corticoendosteal bone formation. Calcif. Tissue Int. 1985; 37:148–156. [PubMed: 3924371]
25. Yang W, Kalajzic I, Lu Y, Guo D, Harris MA, Gluhak-Heinrich J, Kotha S, Bonewald LF, Feng JQ, Rose DW, Harris SE. Identification of an osteocyte-specific mechanically regulated region of the dentin matrix protein 1 gene. J. Biol. Chem. 2005; 280:20680–20690. [PubMed: 15728181]
26. Gu SM, Thompson DA, Srikumari CR, Lorenz B, Finckh U, Nicoletti A, Murthy KR, Rathmann M, Kumaramanickavel G, Denton MJ, Gal A. Mutations in RPE65 cause autosomal recessive childhood-onset severe retinal dystrophy. Nat. Genet. 1997; 17:194–197. [PubMed: 9326941]
27. Pfaffl MW. A new mathematical model for relative quantification in real-time RT-PCR. Nucleic Acids Res. 2001; 29:e45. [PubMed: 11328886]
28. Stern AR, Stern MM, Van Dyke ME, Jähn K, Prideaux M, Bonewald LF. Isolation and culture of primary osteocytes from the long bones of skeletally mature and aged mice. Biotechniques. 2012; 52:361–373. [PubMed: 22668415]
29. Fajardo RJ, Muller R, Ketcham RA, Colbert M. Nonhuman anthropoid primate femoral neck trabecular architecture and its relationship to locomotor mode. Anat. Rec. 2007; 290:422–436.
30. Fajardo RJ, De Silva JM, Manorharan R, Schmitz JE, MacLatchy LM, Bouxsein ML. Lumbar vertebral body bone microstructural scaling in small to medium-sized strepsirhines. Anat. Rec. 2013 Epub ahead of print.
31. Deng Y, Chen Y, Reuss L, Altenberg GA. Mutations of connexin 26 at position 75 and dominant deafness: essential role of arginine for the generation of functional gap-junctional channels. Hear. Res. 2006; 220:87–94. [PubMed: 16945493]
32. Wang M, Martinez AD, Berthoud VM, Seul KH, Gemel J, Valiunas V, Kumari S, Brink PR, Beyer EC. Connexin43 with a cytoplasmic loop deletion inhibits the function of several connexins. Biochem. Biophys. Res. Comm. 2005; 333:1185–1193. [PubMed: 15979566]
33. Bivi N, Condon KW, Allen MR, Farlow N, Passeri G, Brun LR, Rhee Y, Bellido T, Plotkin LI. Cell autonomous requirement of connexin 43 for osteocyte survival: consequences for endocortical resorption and periosteal bone formation. J. Bone Miner. Res. 2012; 27:374–389. [PubMed: 22028311]
34. Plotkin LI, Manolagas SC, Bellido T. Transduction of cell survival signals by connexin-43 hemichannels. J. Biol. Chem. 2002; 277:8648–8657. [PubMed: 11741942]

35. Siller-Jackson AJ, Burra S, Gu S, Xia X, Bonewald LF, Sprague E, Jiang JX. Adaptation of connexin 43-hemichannel prostaglandin release to mechanical loading. J. Biol. Chem. 2008; 283:26374–26382. [PubMed: 18676366]
36. Kitase Y, Barragan L, Qiang H, Kondoh S, Jiang JX, Johnson ML, Bonewald LF. Mechical induction of PGE2 in osteocytes blocks glucocorticoid-induced apoptosis through both the b-catenin and PKA pathways. J. Bone Miner. Res. 2010; 25:2381–2392.
37. Kalajzic I, Matthews BG, Torreggiani E, Harris MA, Pajevic PD, Harris SE. In vivo and in vitro approaches to study osteocyte biology. Bone. 2012 Epub ahead of print.
38. Gluhak-Heinrich J, Gu S, Pavlin D, Jiang JX. Mechanical loading stimulates expression of connexin 43 in aveolar bone cells in the tooth movement model. Cell Commun. Adhes. 2006; 13:115–125. [PubMed: 16613785]
39. Boyce BF, Xing L. Functions of RANKL/RANK/OPG in bone modeling and remodeling. Arch. Biochem. Biophys. 2008; 473:139–146. [PubMed: 18395508]
40. Liu XH, Kirschenbaum A, Yao S, Levine AC. Interactive effect of interleukin-6 and prostaglandin E2 on osteoclastogenesis via the OPG/RANKL/RANK system. Ann. N. Y. Acad. Sci. 2006; 1068:225–233. [PubMed: 16831922]
41. Ramirez-Yanez GO, Symons AL. Prostaglandin E2 affects osteoblast biology in a dose-dependent manner: an in vitro study. Arch. Oral Biol. 2012; 57:1274–1281. [PubMed: 22480456]
42. Jurado S, Garcia-Giralt N, Diez-Perez A, Esbrit P, Yoskovitz G, Agueda L, Urreizti R, Perez-Edo L, Salo G, Mellibovsky L, Balcells S, Grinberg D, Nogues X. Effect of IL-1beta, PGE(2), and TGF-beta1 on the expression of OPG and RANKL in normal and osteoporotic primary human osteoblasts. J Cell Biochem. 2010; 110:304–310. [PubMed: 20225238]
43. Nakashima T, Hayashi M, Fukunaga T, Kurata K, Oh-Hora M, Feng JQ, Bonewald LF, Kodama T, Wutz A, Wagner EF, Penninger JM, Takayanagi H. Evidence for osteocyte regulation of bone homeostasis through RANKL expression. Nat. Med. 2011; 17:1231–1234. [PubMed: 21909105]
44. Xiong J, Onal M, Jilka RL, Weinstein RS, Manolagas SC, O'Brien CA. Matrix-embedded cells control osteoclast formation. Nat. Med. 2011; 17:1235–1241. [PubMed: 21909103]
45. Taylor AF, Saunders MM, Shingle DL, Cimbala JM, Zhou Z, Donahue HJ. Mechanically stimulated osteocytes regulate osteoblastic activity via gap junctions. Am. J. Physiol. Cell Physiol. 2007; 292:C545–C552. [PubMed: 16885390]

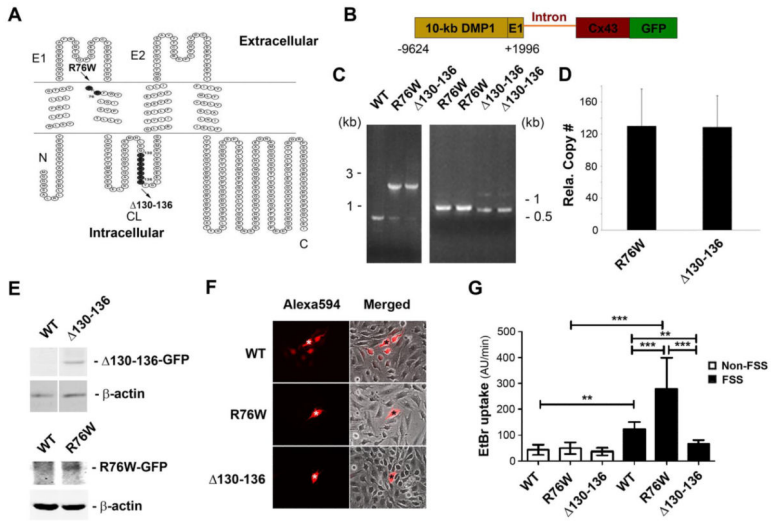

Figure 1. Generation of two transgenic mouse models overexpressing Cx43 mutants

(A) The membrane topological structure of Cx43 was generated by Microsoft Office Visio. R76W mutant (amino acid residue arginine-76 (R) is replaced by tyrosine (W)) (indicated by solid black circle) is located in the interface of second transmembrane and first extracellular loop domain. Δ130-136 mutant (deletion of amino acid residues 130 to 136) is located in the cytoplasmic loop domain. N, NH_2-terminus; C, COOH-terminus; E1, first extracellular loop domain; E2, second extracellular loop domain; CL, cytoplasmic loop domain. **(B)** The DNA constructs used to generate two transgenic mouse models consist of 10-kb DMP1 promoter and exon 1 (E1), and followed by an intron, a full-length Cx43 dominant negative mutant and GFP. **(C)** Genome DNA was extracted from tails of WT and the two transgenic mice. A PCR product of 770 bp pointed to endogenous Cx43 in WT mice and an 1813 bp and 1833 bp to R76W and Δ130-136 mice, respectively (left panel). A size difference of 20 bp was detected between R76W and Δ130-136 mutants (right panel). **(D)** The gene copy numbers were determined using qPCR using genomic DNA isolated from tails of two homozygous transgenic mice. **(E)** Lysates of tibial bone from WT and the two transgenic mice were prepared and immunoblotted with anti-GFP or anti-β-actin antibody followed by corresponding HRP-conjugated goat anti-rabbit or anti-mouse secondary antibody. **(F)** The primary osteocytes were isolated from WT and the two transgenic mice, and were microinjected with Alexa594 dye. Gap junction intercellular coupling was blocked in osteocytes from the two transgenic mouse models, but not from WT mice. The original injected cell was indicated by "*". **(G)** The primary osteocytes were isolated from WT and the two transgenic mice, then were subjected to flow shear stress (FSS) for 15 min or non-FSS conditions. Dye-uptake assay was performed with ethidium bromide (EtBr). Hemichannel dye uptake was only blocked in Δ130-136 mice, but elevated in osteocytes from R76W mice compared to WT. Data shown are mean ± SD. **, $P < 0.01$; ***, $P < 0.001$.

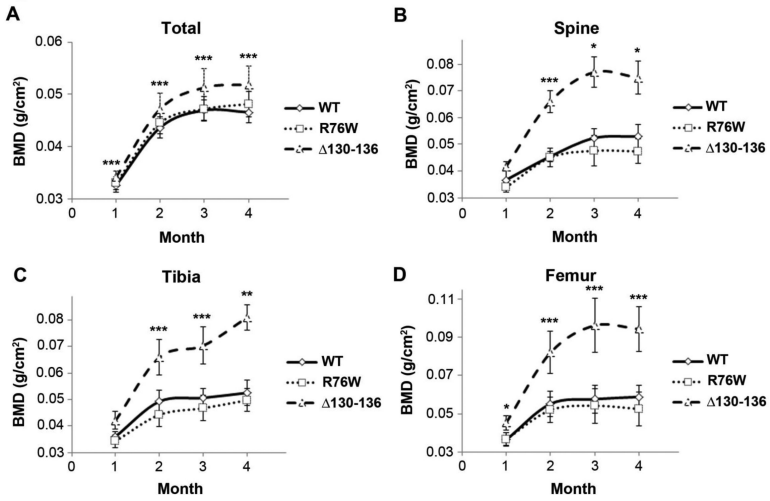

Figure 2. Increased BMD in Δ130-136, but not in R76W, transgenic mice

Total **(A)**, spine **(B)**, tibia **(C)**, and femur **(D)** BMD was measured by DEXA analysis in 1, 2, 3 and 4 month-old, male WT and transgenic mice. As compared to that in WT mice, BMD was significantly elevated in Δ130-136 mice, whereas no significant difference was detected in R76W mice. Data shown are mean ± SD. Δ130-136 versus WT, *, $P < 0.05$; **, $P < 0.01$; ***, $P < 0.001$. n = 19 (WT), 19 (R76W) and 12 (Δ130-136).

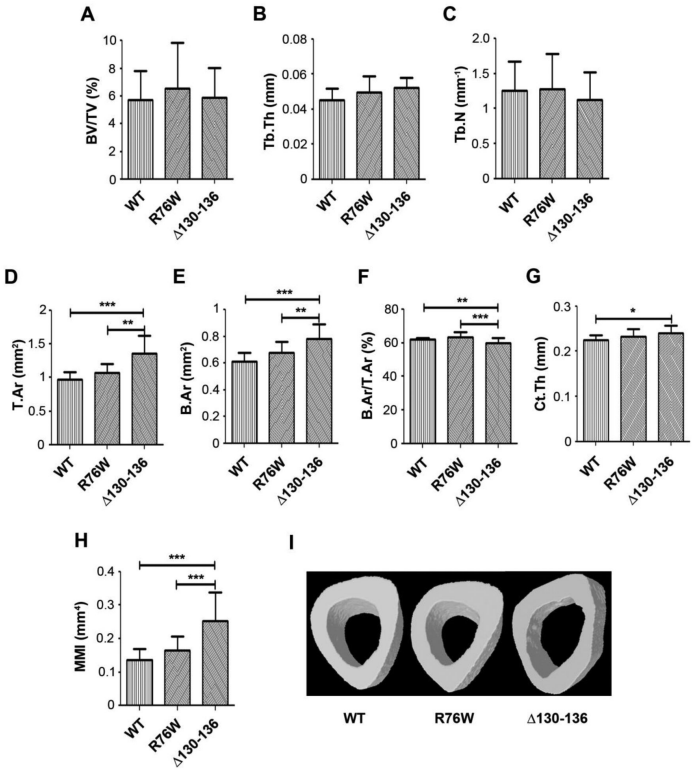

Figure 3. Alterations of bone structure in Δ130-136 transgenic mice as shown by MicroCT analysis

3D microCT analysis of tibial trabecular bone showed that bone volume fraction (BV/TV, **A**), trabecular thickness (Tb. Th, **B**) and trabecular number (Tb. N, **C**) were not significantly different between R76W and Δ130-136 transgenic mouse lines and WT control. MicroCT analysis of tibial midshaft cortical bone showed that total area (T.Ar, **D**), bone area (B.Ar, **E**), cortical thickness (Ct. Th, **G**) and MMI (**H**) were significantly increased in Δ130-136 mice in comparison to WT and R76W mice, while the ratio of B.Ar to T.Ar **(F)** was significantly decreased in Δ130-136 mice compared to WT and R76W mice. Data shown are mean ± SD. *, $P < 0.05$; **, $P < 0.01$; ***, $P < 0.001$. n = 11-17. The microCT images of cross sections of tibial midshaft cortical bone are shown (**I**).

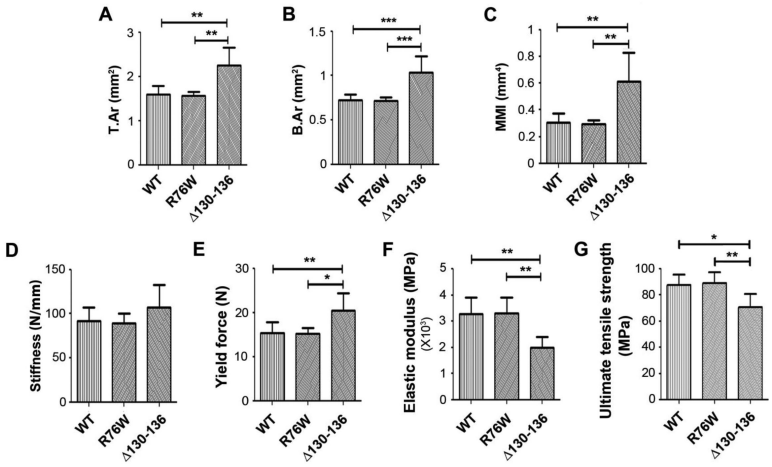

Figure 4. Alterations of bone structure shown by MicroCT are correlated with the changes of bone material properties in Δ130-136 transgenic mice by three point bending analysis

MicroCT analysis of femur midshaft cortical bone showed that total area (T.Ar, **A**), bone area (B.Ar, **B**) and MMI (**C**) were significantly increased in Δ130-136 mice in comparison to WT and R76W mice. Data shown are mean ± SD. **, $P < 0.01$; ***, $P < 0.001$. n = 11-17. Three-point bending assay was performed on isolated femur bones of 4-month old, male WT and transgenic mice, and stiffness **(D)**, yield force **(E)**, elastic modulus **(F)** and ultimate tensile strength **(G)** were measured. Yield force **(E)** was significantly greater in Δ130-136 mice compared to WT and R76W mice. A significant reduction was observed in the elastic modulus **(F)** and ultimate tensile strength **(G)** of Δ130-136 compared to WT and R76W mice. Data shown are mean ± SD. *, $P < 0.05$; **, $P < 0.01$. n = 6.

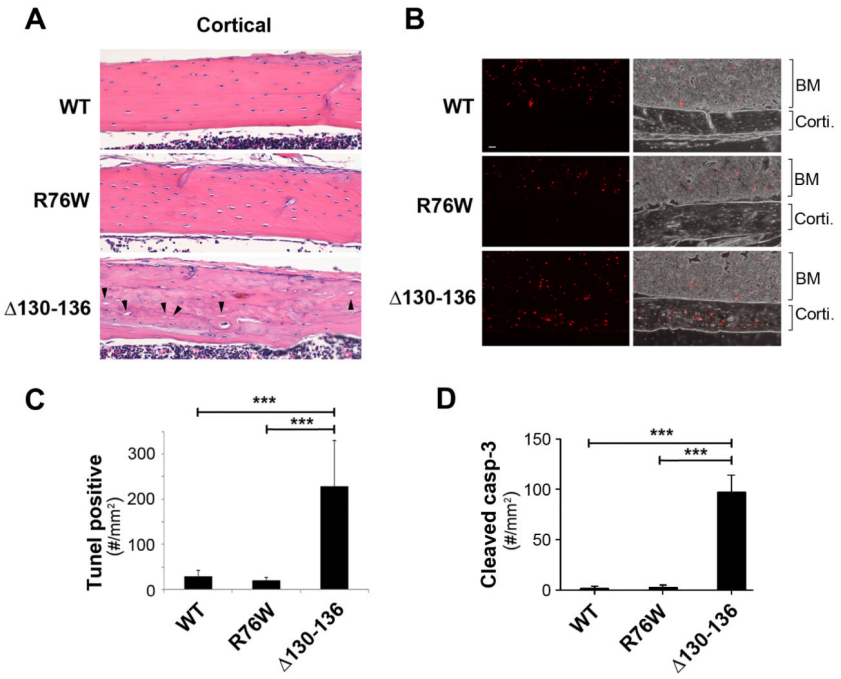

Figure 5. Apoptotic osteocytes and empty lacunae are increased in trabecular and cortical tibial bone of Δ130-136 mice

(A) H&E staining of paraffin sections of 4-month-old tibial bones showed increased numbers of empty lacunae relative to total lacunae in tibial cortical bone in four-month-old Δ130-136 mice, but minimal differences in WT as compared to R76W mice. The solid arrowheads point to the empty lacunae. **(B)** Paraffin sections of 4-month-old tibial bones were TUNEL stained showing fluorescence TUNEL images (left panels) and overlay corresponding fluorescence and phase images (right panels). A significant increase of TUNEL signals was detected in cortical bone area (corti) of Δ130-136 mice, but not much in that of WT and R76W mice. Comparable TUNEL signals were detected in bone marrow (BM) of WT and two transgenic lines. **(C)** The TUNEL signals per mm^2 of cortical bone area were quantified. **(D)** Paraffin sections of 4-month-old tibial bones were immunolabeled with anti-cleaved caspase-3 antibody and the numbers of cleaved caspase-3-positive osteocytes per mm^2 of cortical bone area was quantified. Data shown are mean ± SD. ***, $P < 0.001$. n = 3.

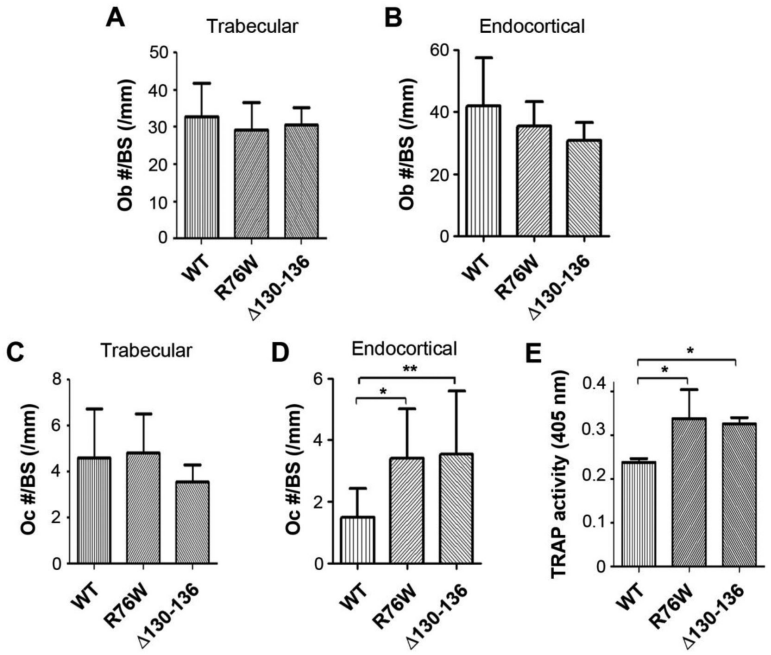

Figure 6. The decreased numbers of osteoblasts, and increased numbers of osteoclasts and osteoclastogenesis in R76W and Δ130-136 transgenic mice

Tibial bones were isolated from four-month-old mice and fixed. The plastic sections were prepared, and osteoblast (**A** and **B**) and osteoclast numbers (**C** and **D**) in trabecular and endocortical bones were quantified using Bioquant Image Analysis System. Data shown are mean ± SD. *, $P < 0.05$; **, $P < 0.01$. (**E**) TRAP activity was assessed at 405 nm in cultures derived from the total bone marrow and induced with RANKL for overnight to promote osteoclastogenesis. Marrow from both Δ130-136 and R76W mice resulted in a significantly higher TRAP activity compared to WT. Data shown are mean ± SD. *, $P < 0.05$. n = 5-7.

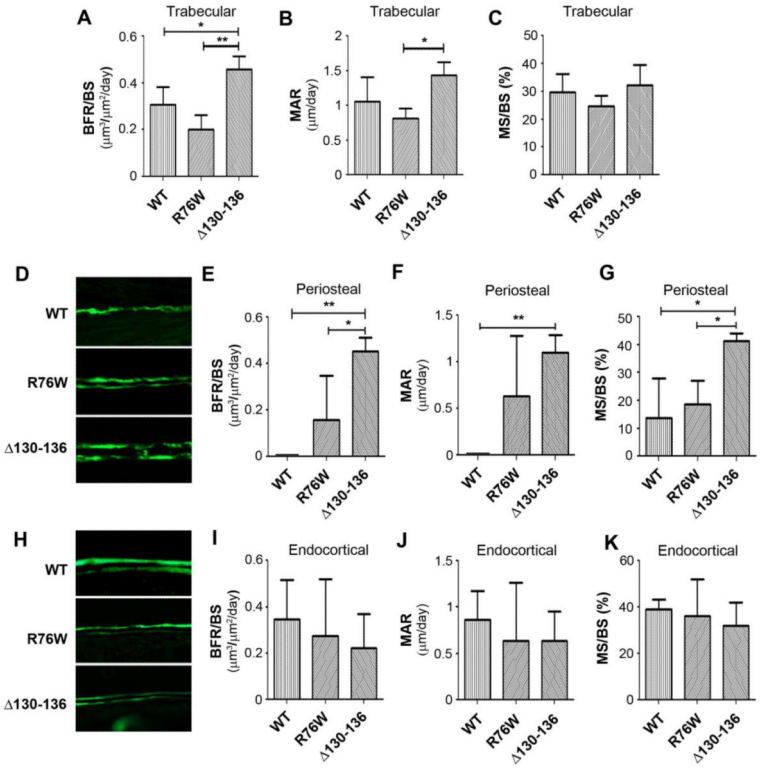

Figure 7. Increased bone formation rate in periosteal bone of Δ130-136 transgenic mice

Four-month-old WT and transgenic mice were injected twice with calcein dye, tibial bones were isolated and plastic sections were prepared. The images of were shown. The dynamic bone histomorphometric parameters were measured in both trabecular (**A-C**), periosteal (**D-G**) and endocortical bones (**H-K**); the calcein double labeling of tibial midshaft cortical bone (**D** and **H**), bone formation rates (BFR/BS, **A, E** and **I**), mineral apposition rates (MAR, **B, F** and **J**) and ratio of mineral surface (MS) to bone surface (BS) (**C, G** and **K**). Data shown are mean ± SD. *, $P < 0.05$; **, $P < 0.01$. n = 3.

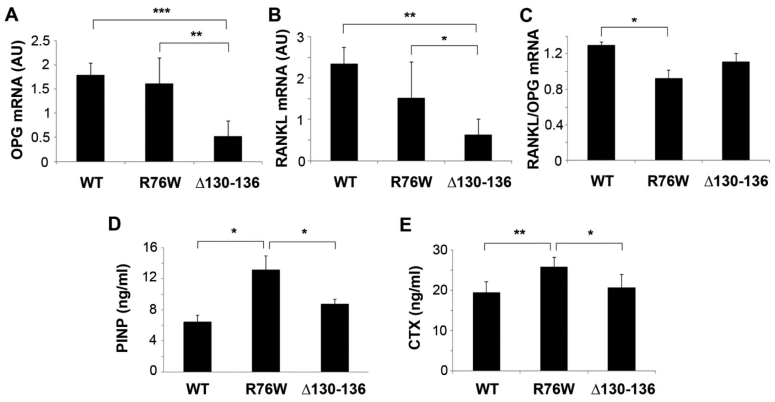

Figure 8. Changes of markers of bone remodeling in transgenic models

(**A**-**C**) Total RNA were extracted from cortical bones of WT and two transgenic mouse models, and were used for RT-PCR analysis probed with primers for OPG and RANKL. mRNA expression of OPG (**A**) and RANKL (**B**) was significantly decreased in Δ130-136 compared to WT and R76W mice, while RANK/OPG ratio (**C**) was reduced in R76W mice compared to WT. (**D** and **E)** Sera were collected from WT and two transgenic mouse models, and the concentration of PINP (**D**) and CTX (**E**) was determined by ELISA assay. The contents of both PINP and CTX were significantly increased in R76W mice as compared to WT and Δ130-136 mice. Data shown are mean ± SD. *, $P < 0.05$; **, $P < 0.01$; ***, $P < 0.001$. n = 6.

TABLE 1

The list of DNA primers used in the paper.

Name	Sequence
TransG-F	5'-ATGGTGAGCAAGGGCGAGGAG-3'
TransG-R	5'-CGGCGGCGGTCACGAAC-3'
mC×43 S-F	5'-CCCGGTTGTGAAAATGTCTGCTAT-3'
mC×43 S-R	5'-CCGGTGGTGGCGTGGTAAG-3'
mC×43 1201-F	5'- CGGAAGCACCATCTCCAACT-3'
mC×43 1310-R	5'- CCACGATAGCTAAGGGCTGG-3'
mC×50, 1272-F	5'- CAAGGGCTGTCTGCTGAGAA-3'
mC×50 1384-R	5'- AGATCATCTGACCTGGCCCT-3'
OPG-F	5'- CTGAGTGAGAACAGAGGGTA-3'
OPG-R	5'-CAAATCAAATCTTTAGAGGG-3'
RANKL-F	5'-ATGAAACTCACAGCCCTCT-3'
RANKL-R	5'-ATAAGCATCGGAATACCTC-3'